ACS APPLIED POLYMER MATERIALS

pubs.acs.org/acsapm

Article

Nanoparticle Mediated Improved Crystallinity and Connectivity of Semiconducting Polymer Thin Films

Md Saifuddin, Arindam Biswas, Saugata Roy, Subhankar Mandal, and Satyajit Hazra*

Cite This: ACS Appl. Polym. Mater. 2023, 5, 3359−3369

Read Online

ACCESS | Metrics & More | Article Recommendations | Supporting Information

ABSTRACT: Polymer nanocomposites (PNCs), i.e., nanoparticle (NP) incorporated semiconducting polymers (SPs), constitute a class of active materials where the dispersion and locations of the NPs and the crystallinity of the SPs play important roles in deciding their device performances. Herein Au nanoparticle (AuNP) mixed poly(3-hexylthiophene) [P3HT] was taken as a model PNC system, and a unique combination of complementary techniques was utilized to address these dispersion-related structural issues, viz the organization and/or dispersion of AuNPs, its evolution with thermal annealing (TA), and their effects on the ordering or crystallization of the P3HT matrix. The layering of AuNPs near the interfaces, namely confined or near monolayer thick layer at the film−substrate interface and fluctuated or near bilayer thick layer at the film−air interface, are evident in the as-cast PNC thin films, indicating self-organization and phase separation tendencies of the similar and dissimilar materials (i.e., dominant decrease of enthalpic energy over entropy) and different (hard and soft) boundary conditions of the interfaces. On the other hand, appreciable dispersion of AuNPs inside P3HT matrix is evident after TA, suggesting thermal energy induced diffusion of AuNPs through amorphous P3HT regions, overcoming the self-organization and phase separation (i.e., dominant increase of entropic energy over enthalpy). Such dispersion enhances the quantity (fraction or amount) and quality (planarity or conjugation length) of P3HT crystallites (and thus validates the dispersion of AuNPs in the amorphous P3HT regions) and their edge-on orientation and connectivity. This information or understanding is very useful for optimizing the structures of the PNC-based active layers for their better charge carrier mobility and device performances.

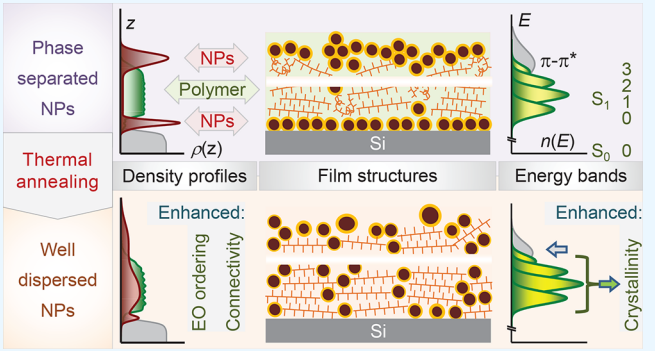

KEYWORDS: *semiconducting polymers, polymer nanocomposites, nanoparticle dispersion, crystallization, edge-on oriented ordering, connectivity*

INTRODUCTION

Semiconducting organic molecules and polymers open an alternate path for the development of devices featuring low cost, easy fabrication, light weight, and high flexibility.[1−4] Owing to the solution processing ability and commercial prospect, poly(3-hexylthiophene) [P3HT] has been studied extensively as one of the more promising semiconducting polymers for organic thin-film transistors (OTFTs).[5−7] However, P3HT forms a semicrystalline morphology consisting of crystalline and amorphous regions. Hence, the orientation (edge-on or face-on), amount (fraction of crystallites), and quality (planarity, local order, and average conjugation length) of the crystalline aggregates and the interconnection between the aggregates, especially near the film−substrate interface, play significant roles in tuning the charge carrier mobility.[8−10] On the other hand, nanomaterials (NMs), like nanoparticles (NPs) or nanorods (NRs), are space-confined objects, which show distinguishing properties as compared to their bulk counterpart.[11,12]

Polymer nanocomposite (PNC), formed by blending NMs with polymer, constitute a class of advanced material, which exhibit distinctive properties relative to the pristine polymer.[13,14] However, a bottleneck in gaining such distinctive properties of PNC is the lack of dispersion of the NMs in the polymer matrix, as NMs are quite often separate out from polymer to minimize the free energy of the system. Hence, a massive amount of research work has been carried out on PNCs to understand and improve the nature of dispersion of NMs in the polymer matrix and their effect on the observed physical properties.[15,16] Also, various strategies have been employed to enhance the dispersibility of various NMs in PNCs, namely tuning the enthalpic and entropic interactions,

Received: January 8, 2023
Accepted: March 30, 2023
Published: April 10, 2023

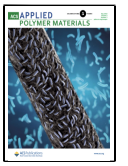

https://doi.org/10.1021/acsapm.3c00049
ACS Appl. Polym. Mater. 2023, 5, 3359−3369

in general and grafting the NMs with polymer chains, in particular.[14,17−19]

In the case of PNC comprising a semicrystalline semiconducting polymer, the organization or spatial dispersion of NMs within self-assembled semicrystalline system itself is a topic of great interest to the scientific community for the development of functional hybrid materials,[20−24] and also for the improvement of its power conversion efficiencies and charge transport properties. Recently, ZnO, TiO_2, CdSe, and Au NMs have been utilized in the P3HT-based organic solar cells to increase their power conversion efficiencies.[25−28] Also, attempts are on to understand the effect of different NMs on the charge transport properties of P3HT-based OTFTs.[29−33] In particular, large number of investigations have already been carried out for the P3HT-AuNM system;[29,32,34] even then the effects of AuNMs on the charge transport properties and device performances are not very clear. This is primarily due to the lack of information about the dispersion and locations of the NMs in the film.

The locations of the dispersed conducting NMs in the PNC film are of prime importance in deciding its device performances. For example, the locations of the NMs in the amorphous polymer regions can establish better contacts between crystallites and also can improve the overall crystallinity (in terms of quantity and quality) of the polymer matrix, both of which in turn can enhance the charge carrier mobility of the system.[29,32] Such information, which are of utmost importance, can be extracted using complementary X-ray reflectivity (XR) and optical absorption techniques.[35,36] XR is capable of providing electron density profile (EDP), i.e., in-plane (x−y) average electron density as a function of depth (z),[37−40] from which information about the aggregation and/or distribution of NMs along depth[18,41,42] and the layering due to ordering of polymer can be obtained,[43−45] while the optical absorption is capable of providing information about the intra- and interchain ordering, the conjugation length, and the percentage of crystalline polymer aggregates in the system.[35,36,46] However, such characterization of PNC thin films containing semiconducting polymers using complementary techniques, in general and XR technique, in particular, through nondestructive ways, are very rare.

In this article, complementary techniques, namely XR, atomic force microscopy (AFM), and optical absorption, were utilized to understand the organization and/or dispersion of AuNPs within P3HT-based PNC thin films, its evolution with thermal annealing (TA), and their effects on the ordering or crystallization of the P3HT matrix. Indeed, the layering of AuNPs near the interfaces are evident in the as-cast PNC thin films, indicating self-organization and phase separation of AuNPs and P3HT, while the dispersion of AuNPs within P3HT matrix is evident after TA indicating the thermal energy induced diffusion of AuNPs overcoming such organization and phase separation. Furthermore, the dispersion of AuNPs is found to enhance the crystallinity and edge-on oriented (EO) ordering of the P3HT matrix. Such NP-induced partial conversion of amorphous P3HT to crystallites suggests that the dispersed-NPs are essentially placed in the amorphous P3HT regions. The improvement of P3HT crystallites and their EO ordering and connectivity in the films, through the dispersion and placement of AuNPs in the amorphous regions of the P3HT matrix, are quite interesting and should have strong implication on the charge carrier mobility of such PNC thin films.

EXPERIMENTAL SECTION

Preparation of P3HT-AuNP Composite Thin Films. P3HT (of average molecular weight 54,000−75,000 and regioregularity >98%), hydrogen tetrachloroaurate trihydrate [$HAuCl_4{\cdot}3H_2O$], sodium borohydride [$NaBH_4$], dodecanethiol [$C_{12}H_{25}SH$] and tetraoctylammonium bromide [$C_{32}H_{68}BrN$] were obtained from Sigma-Aldrich and used as received. Milli-Q water (Millipore) and toluene (Merck) were used as solvents. Dodecanethiol-encapsulated Au nanoparticles (AuNPs) were synthesized by a phase-transfer redox reaction mechanism using the Brust method,[47] the details of which were reported before.[48] The mean diameter of the particles, as obtained from the TEM analysis (shown in Figure S1 of the Supporting Information), is about 2.0 ± 0.5 nm for the bare AuNP and 4.0 ± 0.5 nm for the thiol coated AuNP.

Solutions of different concentration and/or weight ratio (R_M) of P3HT and AuNPs were first prepared by dissolving different amount (M) of P3HT and AuNPs in 1 mL of toluene as shown in Table 1.

Table 1. PNC Thin Film Specification Showing the Amount of P3HT (M_P) and AuNPs (M_{NP}) in 1 mL of Toluene and Their Ratio (R_M) in the Solution

sample	M_P [mg]	M_{NP} [mg]	R_M
PN30	4.00	0.00	1:0
PN10	2.50	0.00	1:0
PN31	4.00	1.34	3:1
PN32	2.40	1.60	3:2
PN11	2.50	2.50	1:1

The solutions were then sonicated for 5 min and annealed at 60 °C for 5 min. Prior to the film deposition, Si and quartz glass wafers (of size about 12 × 12 mm^2) were sonicated in acetone and ethanol to remove organic contaminates. Pure P3HT and PNC thin films (as shown in Table 1) were then formed on Si and quartz glass substrates using a spin-coater (SCS 6800) at fixed spinning speed (1000 rpm) and time (60 s).[35] All films were subsequently annealed at 70 °C for 15 min under vacuum condition, which are referred to as as-cast films. Films were also heated at different temperatures for a fixed duration under a vacuum condition, and the characterizations were carried out during and after TA, which are referred to as *in situ* and *ex situ* TA.

Characterization of P3HT-AuNP Composite Thin Films. The *ex situ* XR measurements of the films after TA were performed using a versatile X-ray diffractometer (VXRD, D8 Discover, Bruker AXS) setup with Cu Kα radiation (of λ_X = 1.54 Å),[49−51] while the *in situ* XR measurements of the films during TA were carried out using a synchrotron source (MCX beamline, Elettra) at an energy 10 keV (i.e., wavelength, λ_X = 1.24 Å).[35,52] XR data were taken in specular condition; i.e., the incident angle is equal to the reflected angle (θ), and both are in a scattering plane. Under such a condition, there exists a nonvanishing wave vector component, q_z, which is given by $(4\pi/\lambda_X)$ sin θ.

Topography of the PNC thin films (before and after TA) were mapped by an atomic force microscope (CSI Nano-Observer).[35,53] Topographic images were collected using Au coated Si tip (radius of curvature ∼10 nm) in a tapping mode (resonance frequency ∼60 kHz) to minimize tip-induced damage of the soft film. Scans of different sizes and in different portions of the sample were carried out to get statistically meaningful information about the topography. Processing and analysis of AFM images were carried out using Gwyddion software. Optical (UV−vis) absorption spectra of the PNC thin films on quartz glasses (before and after TA at different temperatures) were collected using a UV−vis spectrophotometer (JASCO, V-630).[35,36]

RESULTS AND DISCUSSION

XR and Out-of-Plane Structures. Effect of *Ex Situ* Thermal Annealing. XR profiles, normalized by Fresnel reflectivity (R_F), for two PNC (PN31 and PN11) thin films,

https://doi.org/10.1021/acsapm.3c00049
ACS Appl. Polym. Mater. 2023, 5, 3359−3369

before and after TA (at different temperatures), obtained using a laboratory X-ray source, are presented in Figure 1. A

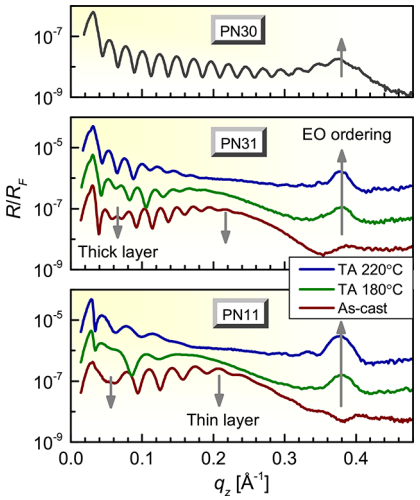

Figure 1. Evolution of normalized XR profiles (different symbols) and analyzed curves (solid lines) of PNC thin films with different amount of AuNPs and after different TA. Curves are shifted vertically for clarity. The presence of thick and thin layer-related modulations, in addition to the EO ordering related peak, in the XR profiles of the PNC thin films and their evolution with TA is indicated.

normalized XR profile of the as-cast P3HT (PN30) thin film is also included in Figure 1, for comparison. The presence of Kiessig fringes (measure of film thickness) of decaying amplitude (signature of roughness) and a pseudo Bragg peak near $q_z \approx 0.38$ Å^{-1} (signature of EO ordering) are evident in all the films. In addition, the presence of thick and thin layer-related modulations near $q_z \approx 0.06$ and 0.21 Å^{-1} is also clearly evident in the XR profiles of the as-cast PNC thin films. The modulation or broad hump near $q_z \approx 0.21$ Å^{-1} is indicative of a thin layer of thickness around 3 nm, which is well correlated with the monolayer of AuNPs. This indicates presence of a monolayer thick AuNP layer within as-cast PNC thin film, the coverage of which increases with the amount of AuNPs. The intensity of the hump is found to diminish with TA and completely vanishes after TA at 220 °C, indicating thermal energy driven destruction of such monolayer structure. The modulation near $q_z \approx 0.06$ Å^{-1} also vanishes completely after TA at 220 °C. On the other hand, the Bragg-peak for both the films becomes prominent with TA, indicating thermal energy driven enhancement of the EO ordering.

To get more quantitative information about the out-of-plane organization of AuNPs within P3HT matrix, the XR data of the PN31 and PN11 thin films, as shown in Figure 2, were analyzed using matrix method after incorporating roughness at each interface.[38,54] During data analysis, an instrumental resolution in the form of a Gaussian function and a constant background were also included.[41] For the analysis, each film above the substrate (Si/SiO_2) was divided into a number of layers. It was observed that 3-layer model, namely high-density low-thickness bottom layer (L_b) of AuNPs, low-density high-thickness middle layer (L_m) of P3HT or AuNP-mixed P3HT, and high-density intermediate-thickness top layer (L_t) of AuNPs, can very well generate the Keissig fringes and their modulations near $q_z \approx 0.06$ and 0.21 Å^{-1}, as observed in the XR profiles of the as-cast PNC thin films. To generate the pseudo Bragg peak, the middle layer was considered as a repetition of bilayers, where each bilayer of thickness d consists of high electron density (ρ_{bb}) polythiophene backbone layer of thickness d_{bb} and low electron density (ρ_{sc}) alkyl side chain containing layer of thickness d_{sc} plus a constant background arising from amorphous P3HT and/or diffused AuNPs, similar to that reported before.[35] This gives rise an electron density contrast of $\Delta\rho = \rho_{bb} - \rho_{sc}$ over the average electron density due to EO ordering of the P3HT. The information of the critical wave-vector of the film ($q_{c,film}$), as shown in the zoomed view of the selected portion of the XR profile in Figure 2, was used to estimate the average density of film (ρ_a). Also, conservation of materials after TA of the film was considered and checked, by measuring the area under the EDP (i.e., $\int \rho(z)\, dz$) after each step of data analysis,[41] to find out the most feasible solution.

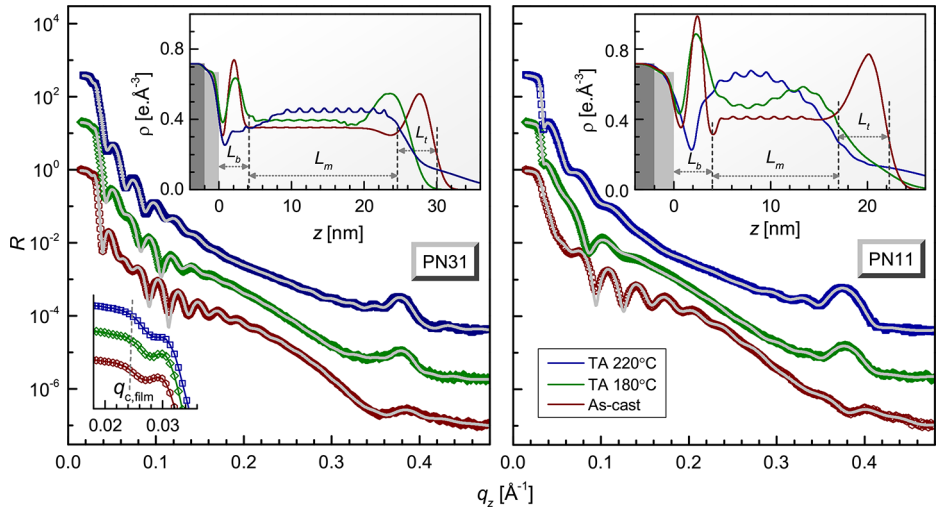

Figure 2. Evolution of XR profiles (different symbols) and analyzed curves (solid lines) of two PNC thin films of different amount of AuNPs due to different TA. Bottom inset: Zoomed view of the selected portion of the XR profiles where the positions of the critical wave-vector ($q_{c,film}$) of the film are indicated. Curves are shifted vertically for clarity. Top insets: Corresponding analyzed EDPs showing the evolution of the top, middle and bottom layers in the films with TA.

https://doi.org/10.1021/acsapm.3c00049
ACS Appl. Polym. Mater. 2023, 5, 3359−3369

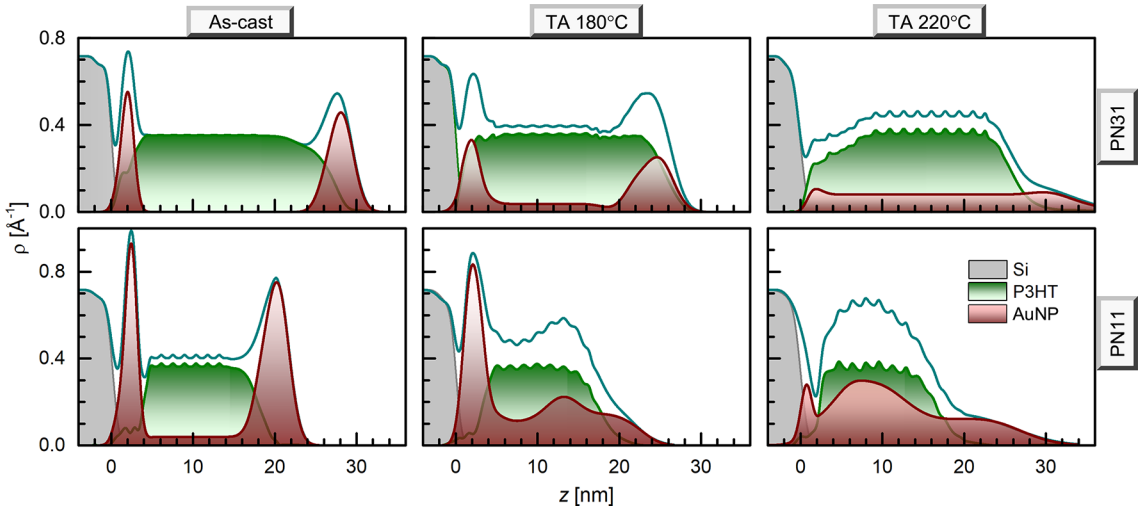

Figure 3. Deconvoluted EDPs of two PNC (PN31 and PN11) thin films before and after TA (at different temperatures), showing the location, amount, organization, and evolution of P3HT and AuNPs in the films.

Table 2. Parameters, Such as the Film Thickness (D), the Integrated Electron Density of P3HT ($\sum\rho_P$) and AuNP ($\sum\rho_{NP}$), the Percentage of $\sum\rho_{NP}$ at Bottom ($\sum\rho_{NP,b}$), Top ($\sum\rho_{NP,t}$), and Middle ($\sum\rho_{NP,m}$), the Maximum Coverage of the AuNP Layer (w.r.t. to Packed Monolayer Coverage) at Bottom (C_b), Top (C_t), and Middle (C_m), the Width (FWHM) of the AuNP Layer at Bottom (w_b) and Top (w_t), the Position of the AuNP Layer at Top (z_t), and the Thickness (d) and the Maximum Electron Density Contrast ($\Delta\rho_P$) of the P3HT bilayer for the PNC Thin Films of Different Compositions and Different Thermal Treatments, as Obtained from the XR Data Analysis

sample	treatment	$\sum\rho_P$, $\sum\rho_{NP}$ [eÅ^{-2}]	D [nm]	$\sum\rho_{NP,b}$ [%]	C_b [%]	w_b [nm]	$\sum\rho_{NP,t}$ [%]	C_t [%]	w_t [nm]	z_t [nm]	$\sum\rho_{NP,m}$ [%]	C_m [%]	d [nm]	$\Delta\rho_P$ [eÅ^{-3}]
PN31	as-cast	87 and 29	29.4	38	42	2.0	62	35	4.2	28	0	0	1.64	0.002
	TA 180 °C		26.3	33	25	2.6	50	19	5.4	25	17	3	1.65	0.007
	TA 220 °C		25.8	10	8	3.2	26	9	8.4	31	64	7	1.69	0.023
PN11	as-cast	54 and 54	21.7	35	70	1.8	55	57	3.8	20	10	3	1.42	0.015
	TA 180 °C		17.7	35	60	2.2	22	10	7.5	19	43	15	1.61	0.020
	TA 220 °C		17.0	10	20	2.0	22	9	9.6	22	68	20	1.64	0.030

The best fit XR profiles and the corresponding EDPs for the PN31 and PN11 thin films thus obtained are presented in Figure 2. The presence of high density layers (of AuNPs) at two interfaces of the as-cast films are evident from the analyzed EDPs, which due to TA decreases to increase the overall density of the film, suggesting thermal energy driven interdiffusion of AuNPs. To get further information about the dispersion of AuNPs in the film and its effect on the EO ordering of P3HT, the analyzed EDPs were deconvoluted in terms of AuNPs and P3TH, considering the ratio of integrated electron densities of P3HT ($\sum\rho_P$) and AuNPs ($\sum\rho_{NP}$) as R_M and the materials are independently conserved during the thermal treatment process. Such deconvoluted EDPs for the two PNC thin films before and after TA are shown in Figure 3. The relevant parameters, such as the distributed amount of AuNPs (in percentage) at bottom ($\sum\rho_{NP,b}$), top ($\sum\rho_{NP,t}$), and middle ($\sum\rho_{NP,m}$) of the film, the maximum coverage of AuNPs (in percentage, considering $\rho_{NP} \approx 1.3$ eÅ^{-3} represents full or 100% coverage as obtained from Figure S2 of the Supporting Information) at bottom (C_b), top (C_t), and middle (C_m) layers, the width (FWHM) of the bottom (w_b) and top (w_t) AuNP layers (where width of the perfect monolayer of AuNPs is about 1.5 nm as obtained from Figure S2 of the Supporting Information), the position of the top AuNP layer (z_t), and the maximum electron density contrast ($\Delta\rho_P$) within the P3HT layer of thickness d, as obtained from the EDPs and their deconvolution, are listed in Table 2.

It is evident from Table 2 that, in the as-cast PN31 thin film, almost all the AuNPs are either near the film−substrate interface (~38%) within small width ($w_b \approx 2.0$ nm) to have a large coverage ($C_b \approx 42\%$) or near the film−air interface (~62%) within large width ($w_t \approx 4.2$ nm) to have a relatively small coverage ($C_t \approx 35\%$) with nothing in the middle of the film. On the other hand, in the as-cast PN11 thin film, having relatively large amount of AuNPs, though most (~90%) of the AuNPs are either near the film−substrate interface (~35%) within a small width ($w_b \approx 1.8$ nm) to have a very large coverage ($C_b \approx 70\%$) or near the film−air interface (~55%) within a large width ($w_t \approx 3.8$ nm) to have a large coverage ($C_t \approx 57\%$) but some (~10%) are in the middle of the film. The latter enhances the EO ordering of P3HT (as the $\Delta\rho_P$-value changes from ~0.002 to ~0.015 eÅ^{-3}), while the increase in the number of AuNPs in the film decreases the d-value (from ~1.64 to ~1.42 nm). With TA, the values of $\sum\rho_{NP,b}$, C_b, $\sum\rho_{NP,t}$, and C_t are found to decrease, with an increase in the values of $\sum\rho_{NP,m}$ and C_m. In the 220 °C annealed films, appreciable amounts (60−70%) and coverages (7−20%) of AuNPs are found in the middle of the film. In fact, large amount of AuNPs (about 70−80%) are dispersed in the film and the rest (about 20−30%) of the AuNPs remain vertically phase-separated at the top. TA also increases the $\Delta\rho_P$-value (by 0.01−0.02 eÅ^{-3}) and the d-value (by 0.5−2.0 Å).

The formation of AuNP layers only at the interfaces indicates that the interaction between similar materials is

https://doi.org/10.1021/acsapm.3c00049
ACS Appl. Polym. Mater. 2023, 5, 3359−3369

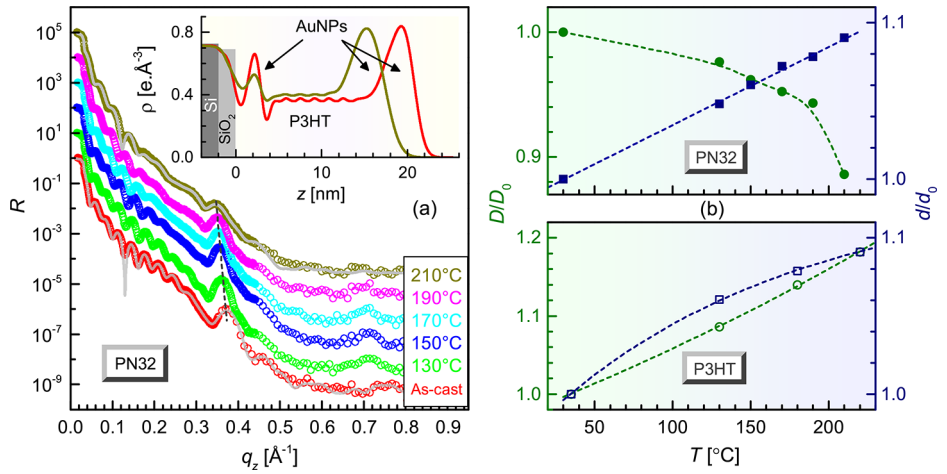

Figure 4. (a) Evolution of in situ XR profiles (symbols) and selected analyzed curves (solid lines) of a PNC (PN32) thin film during annealing at different temperatures. Inset: Corresponding analyzed EDPs showing major locations of AuNPs and P3HT in the film. (b) Evolution of normalized film-thickness (D/D_0) and normalized bilayer-thickness (d/d_0) with in situ annealing temperature (T) for the PNC (PN32) thin film (top) and the polymer (P3HT) thin film (bottom).

different compared to dissimilar materials. Lower thickness or better confinement of the bottom AuNP layer ($w_b \approx 2$ nm, near monolayer) compared to the top layer ($w_t \approx 4$ nm, less than bilayer) suggests strong role of substrate boundary condition. The presence of AuNPs in the middle of the as-cast PN11 film indicates that if the relative amount of AuNPs is high then few can be trapped or dispersed inside P3HT matrix, while the decrease of d-value indicates that the increased number of AuNPs at the interfaces can create pressure to tilt the alkyl side chains within EO crystallites. On the other hand, the decrease in the value of $\sum\rho_{NP,b}$ and $\sum\rho_{NP,t}$, and the increase in the value of $\sum\rho_{NP,m}$ with TA are a signature of thermal energy driven diffusion and dispersion of AuNPs inside P3HT matrix, overcoming attraction from other AuNPs and repulsion from P3HT. This also leads to the decrease in the film thickness and increase in the EO ordering of the film. The presence of phase-separated AuNP layer on the top of the film, even after TA, can be considered as the thermal energy driven agglomeration of AuNPs and subsequent restriction in their diffusion inside the P3HT matrix. The increase the d-value suggests thermal energy induced untilting and/or relaxation of the alkyl side chains.

Effect of *In Situ* Thermal Annealing. The *in situ* evolution of XR profiles of a PNC (PN32) thin film during TA at different temperatures, obtained using synchrotron source, is depicted in Figure 4a. The evolution of the Kiessig fringes (separation) and the pseudo Bragg peak (both position and intensity) with TA are quite evident in all the XR profiles. The values of D and d, normalized with the values of the as-cast film (D_0 and d_0), as obtained from the Kiessig fringes and the pseudo Bragg peak positions, are plotted as a function of annealing temperature (T) in Figure 4b. Such parameters for the P3HT thin film, reported before,[35] are also included in Figure 4b, for comparison. The d/d_0-value of the PNC thin film is found to increase (~10%) with T, similar to the P3HT thin film, while the D/D_0-value of the PNC thin film is found to decrease (~10%) with T, unlike P3HT thin film (where it increases ~20%). The increase in the d-value with T is usually related to the thermal expansion and/or relaxation of the polymer side chains. This usually leads to the increase in the D-value, which is observed in the P3HT thin film but not in the PNC thin film. Even for the P3HT thin film, the increase percentage of the D-value (~20%) is quite high compared to the d-value (~10%), which suggests that other than EO structure also play crucial role in the film thickness. The decrease of D-value for the PNC thin film due to TA, overcoming the 20% thermal expansion observed for the P3HT thin film, indicates appreciable interdiffusion of AuNPs inside P3HT (in the available free volume regions). In fact, such decrease in the thickness helps to validate not only the dispersion of AuNPs inside the P3HT matrix but also in the amorphous regions of the polymer, where maximum free volumes are available. Such decrease is particularly appreciable after 200 °C.

To get further information about the *in situ* evolution of the structure of the PNC thin film, XR profiles of the PN32 thin film are analyzed considering the model that was used before for the PN31 and PN11 thin films. The best fit XR profiles and the corresponding EDPs for the PN32 thin film, before annealing and during annealing at 210 °C, are shown in Figure 4. Appreciable decrease in the values of D, $\sum\rho_{NP,b}$ (or C_b), and $\Delta\rho_P$, and negligible change in the values of $\sum\rho_{NP,t}$ (or C_t) and $\sum\rho_{NP,m}$ (or C_m) are evident with TA. The latter suggests restricted diffusion of AuNPs inside P3HT matrix from the top layer. It is known that the intense synchrotron beam, though useful for obtaining relatively wide dynamic range XR data, can create beam-induced damage in the organic coating of the AuNPs. This in turn can force the AuNPs to agglomerate locally to form large (in-plane elongated disk-like) particles.[55] Such large particles then find it extremely difficult to diffuse inside the matrix, rather can create pressure on the soft P3HT matrix on TA to deteriorate its EO ordering and/or crystallinity and to decrease the film-thickness, as observed.

AFM and Topography. Typical AFM images for a PNC film, before and after TA, are shown in Figure 5, to complement and/or verify the topographic information on the film and its evolution after TA (using real space mapping) with the structural information (as predicted from the reciprocal space mapping). Homogeneous presence of AuNPs, with fluctuation in their heights, is apparent at the surface of the as-cast PNC film (from the different scan-size images). Similar presence of AuNPs is also apparent (from the

https://doi.org/10.1021/acsapm.3c00049
ACS Appl. Polym. Mater. 2023, 5, 3359−3369

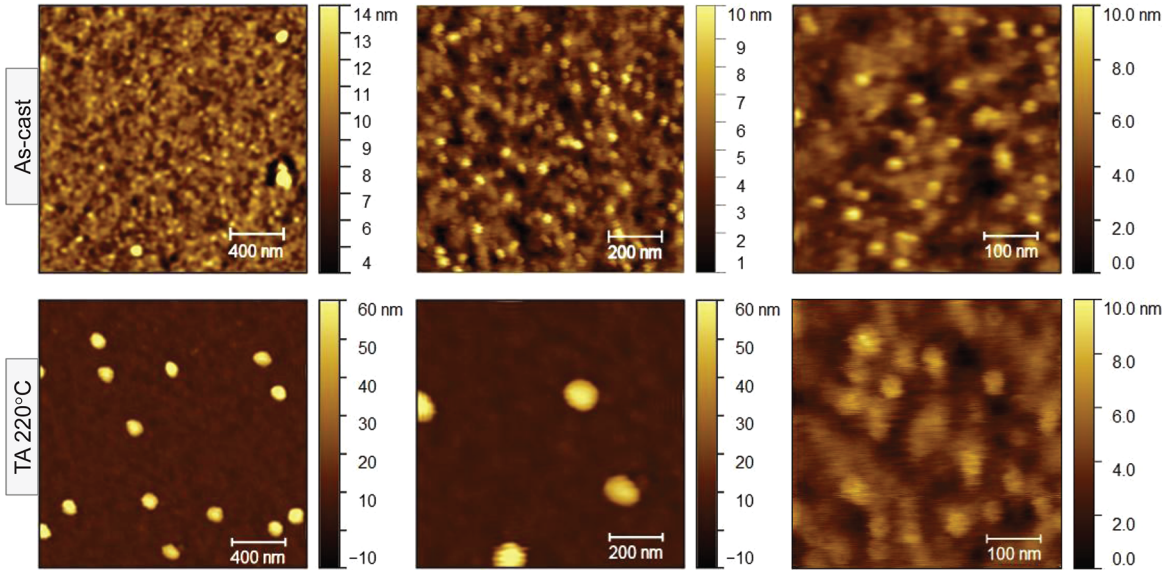

Figure 5. AFM images (in different scan sizes) of a PNC thin film before (as-cast) and after TA, showing the homogeneous presence of fluctuated AuNPs at the surface of the as-cast film and well separated large size islands and relatively smear surface, in between, after TA.

small scan-size images) in the film after TA, though their signature or coverage becomes comparatively weak. In addition, well-separated large (~100 nm) size islands are also visible (from the large scan-size images) in the film after TA.

Further insight about the film topography is obtained from the plot of Minkowski volume (MV) and the surface area (SC) as a function of height (z) (as shown in Figure S3 of the Supporting Information). It is evident from the height histogram that the height fluctuations of the majority of the surface of the film, before and after TA, are similar. The film-surface roughness (σ_t), as estimated from the height histogram, is ~1.2 nm. This value is in good agreement with the value ($\sigma_t \approx 1.0$ nm) obtained from the EDP. On the other hand, the presence of MV, beyond 4 nm height, is evident in the film after TA, which is not present in the as-cast film. The presence of MV or well-separated large size islands, above the average top surface of the film after TA, is a clear indication of the thermal energy driven agglomeration of AuNPs, as inferred before from the EDP.

Optical Absorption and Crystallinity. Optical absorption spectra (normalized with the peak intensity at 540 nm) of two PNC (PN31 and PN11) films, before and after TA (at different temperatures), are presented in Figure 6, to understand the effect of AuNPs and the TA on the degree of intra and interchain ordering of P3HT and the crystalline aggregation.[46,56] The absorption spectra of two P3HT (PN30 and PN10) films are also included (dashed lines) in Figure 6, for comparison. Several peaks in the higher wavelength region (around 500−620 nm) and a broad tail toward lower wavelength region, are evident in all absorption spectra. The intensity and shape of which are found to vary with composition and annealing temperature. The peaks in the higher wavelength region can be attributed to the transitions between states arising from aggregated (crystalline) polymers,[57] whereas the broad tail toward lower wavelength region can be attributed to the transitions between states arising from the disordered polymers.[58]

The transitions between states in the higher wavelength region can be expressed using a series of Gaussian peaks (similar to the Frank−Condon progression) considering crystalline polymers as weakly interacting H-aggregates.[35,59−61] Further, considering the peaks are of same width (σ_c) and equispaced (in energy scale by E_p), the absorption of the crystalline part can be expressed as[36]

$$I_c(\lambda) = \sum_j I_{0-j} \exp\left[-\left\{\left(\lambda - \frac{hc\lambda_{0-0}}{hc + jE_p\lambda_{0-0}}\right)/\sigma_c\right\}^2\right] \quad (1)$$

where I_{0-j} is the intensity and λ_{0-j} is the position of the $0-j$ transition related Gaussian peak, h is Planck's constant, c is the velocity of light, and hc = 1239.8 eV nm.

Similarly, the absorption of the amorphous part can be expressed using a broad Gaussian peak associated with the intrachain $\pi-\pi^*$ transition as[36]

$$I_a(\lambda) = I_{a,0} \exp[-\{(\lambda - \lambda_a)/\sigma_a\}^2] \quad (2)$$

where $I_{a,0}$ is the intensity, λ_a is the position, and σ_a is the width of the Gaussian peak. Accordingly, the contribution of the crystalline and amorphous parts in the absorption can be estimated considering the area under the curves ($A_c = \sqrt{\pi}\sigma_c \sum_j I_{0-j}$ and $A_a = \sqrt{\pi}\sigma_a I_{a,0}$).

In the weakly interacting H-aggregates, due to their interband mixing, the intensity ratio of the 0−0 and 0−1 vibronic lines (I_{0-0}/I_{0-1}) is related to the nearest-neighbor interchain Coulombic coupling ($J_0 > 0$) via the free-exciton bandwidth ($W = 4J_0$) of the aggregates and the energy of the main intramolecular vibration (E_p) coupled to the electronic transition.[46] Assuming a Huang−Rhys factor to be unity,[59,60] W can be expressed as[36]

$$W \approx E_p \frac{1 - \sqrt{I_{0-0}/I_{0-1}}}{0.24 + 0.073\sqrt{I_{0-0}/I_{0-1}}} \quad (3)$$

where an increase in the I_{0-0}/I_{0-1} ratio corresponds to a decrease in the W-value and the excitonic coupling, and therefore an increase in the conjugation length (or planarity) and the degree of intrachain order.[62,63]

https://doi.org/10.1021/acsapm.3c00049
ACS Appl. Polym. Mater. 2023, 5, 3359−3369

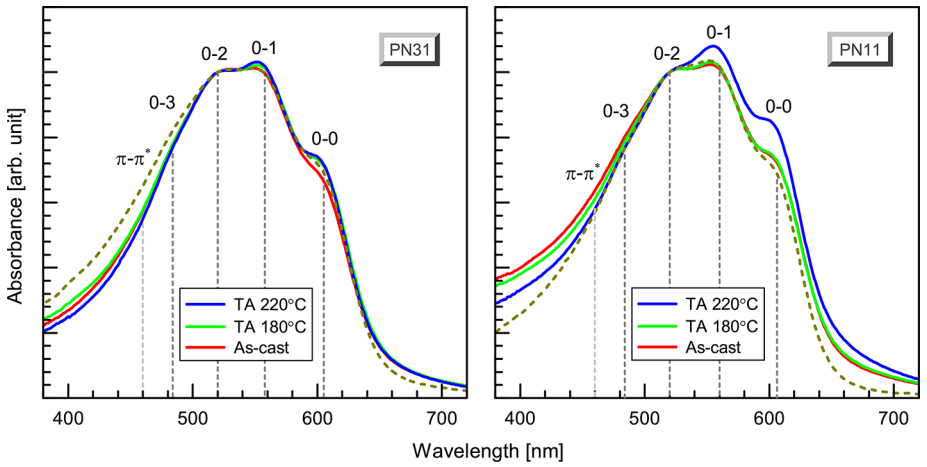

Figure 6. UV−vis spectra (normalized by the 0−2 transition peak intensity) of the PN31 and PN11 thin films before (as-cast) and after TA (at different temperatures). The transition peaks, arising from amorphous (π−π*) and weakly interacting H-aggregates, are indicated. Spectra of the as-cast PN30 and PN10 thin films (dashed line) are also included for comparison.

The optical absorption spectra are simulated using eqs 1 and 2 (shown in Figure S4 of the Supporting Information) and the relevant parameters, namely λ_{0-0}, σ_c, E_p, and the fraction of crystalline aggregates $[f_c = A_c/(A_a + A_c)]$ as obtained from the simulation, are listed in Table 3. The values of W, estimated using eq 3, are also listed in Table 3. The value of E_p, which is due to the C═C symmetric stretch, remains the same (~0.17 eV), while the value of λ_{0-0} (or σ_c) either remains the same or increases (or decreases) due to the AuNPs incorporation and/or thermal treatment of the film. Significant changes in the values of f_c and W are evident (in Table 3) due to the inclusion of AuNPs in the films and their TA.

Table 3. Parameters, Such as the Position (λ_{0-0}) and Width (σ_c) of the 0−0 Transitional Peak, the Intramolecular Vibrational Energy (E_p), the Fraction of Crystalline Aggregates (f_c), and the Exciton Bandwidth (W) for the PNC thin Films of Different Composition and Different Thermal Treatment as Obtained from the Analysis of the Absorption Spectra

sample	treatment	λ_{0-0} [nm]	σ_c [nm]	E_p [eV]	f_c	W [meV]
PN30	as-cast	605	29.9	0.17	0.73	71
PN31	as-cast	605	30.2	0.17	0.77	100
	TA 180 °C	605	29.0	0.17	0.77	86
	TA 220 °C	605	28.7	0.17	0.80	86
PN10	as-cast	605	29.8	0.17	0.74	80
PN11	as-cast	606	28.8	0.17	0.81	75
	TA 180 °C	606	28.8	0.17	0.82	78
	TA 220 °C	606	28.8	0.17	0.83	67

In the as-cast condition, the f_c-values for the PNC (PN31 and PN11) thin films are found large compared to those of the P3HT (PN30 and PN10) thin films. Also, the value of f_c for the PN11 film is found to be more compared to the PN31 film. These results indicate AuNP induced growth of crystalline P3HT aggregates. On the other hand, the value of W for the PN31 film is found to be more compared to the PN30 film, while that for the PN11 film is found to be less compared to the PN10 film, indicating AuNP induced deterioration as well as improvement in the conjugation length or backbone planarity of the polymer aggregates. This can be realized by considering the position dependent role of AuNPs in the W-value, namely deterioration when AuNPs are present near the P3HT interface and improvement when AuNPs are present inside the P3HT matrix. The competitive effects of these two will ultimately decide the final effect or result.

A small increase (or decrease) in the value of f_c (or W) is observed in the PNC thin films after TA (especially after TA at 220 °C). Such an increase in the f_c can be attributed to the thermal energy induced diffusion of the AuNPs inside P3HT matrix and subsequent AuNP induced partial crystallization of the amorphous phase. Similarly, the decrease in the W can be attributed to the thermal energy induced increase in the number of AuNPs inside P3HT matrix, which in turn improves the conjugation length and/or backbone planarity of the polymer aggregates.

Growth, Structure, and Morphology of PNC Thin Films. Let us now try to understand the growth, structure, and morphology of the PNC thin films and their possible implications in the device properties. The overall growth, structure and morphology of the PNC thin films, i.e., the initial structure and morphology and their evolution after TA, can be modeled using the information obtained from the complementary techniques, as shown schematically in Figure 7.

During spin coating, strong or attractive interaction between similar materials and weak or repulsive interaction between dissimilar materials mainly govern the structures. Accordingly, most of the AuNPs are self-organized (through attractive force) and vertically phase separated from P3HT (through resultant repulsive force along the z-direction) to form layered structures at the interfaces, as observed. When the relative amount of AuNPs is high in the solution, then during film growth few of them escape from such a unidirectional repulsive force to trap or disperse inside the P3HT matrix. This can be considered as concentration tuned dispersion of AuNPs in the PNC system. During film deposition, when a mixed solution is placed on the substrate then a gradient in the viscosity along z-direction is formed due to the higher evaporation rate of the solvent from the top surface. This viscosity gradient (namely high viscosity toward top and low viscosity toward bottom) and the repulsive interaction from the substrate surface then forced some of the bottom AuNPs to diffuse toward the top. Accordingly, more number of AuNPs are assembled near the film−air interface compared to the film−substrate interface, as observed. Further, the hard boundary condition of the

https://doi.org/10.1021/acsapm.3c00049
ACS Appl. Polym. Mater. 2023, 5, 3359−3369

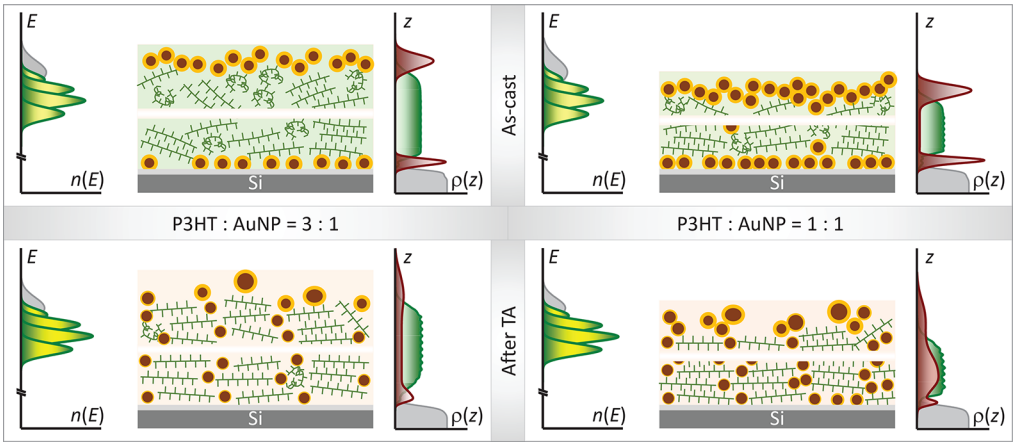

Figure 7. Structural schematics, along with the energy-band diagrams (corresponding to the crystalline P3HT aggregates) and deconvoluted EDPs, of the PNC thin films of different P3HT and AuNP ratios before (as-cast) and after TA, as obtained from the optical absorption, XR, and AFM data analysis, showing the evolution of the phase separation, the organization and dispersion of AuNPs, the amorphous and crystalline natures of P3HT matrix, and the backbone planarity, orientation, and connectivity of the P3HT crystallites.

substrate forced the film−substrate interfacial AuNP layer to become more confined along *z*-direction (to form near monolayer thickness) compared to the film−air interfacial AuNP layer (with more fluctuation to form more than monolayer but less than bilayer thickness). The presence of AuNP layers at the interfaces can reduce the contact resistance and the charge injection barrier between electrode and P3HT layer for both top-contact and bottom-contact OTFT devices, if Au is used as electrode material,[31] which are useful to enhance their charge carrier mobility.

The layering of AuNPs near substrate was also observed before in the PNC films containing insulating polymer like polystyrene but only after the thermal annealing.[64] Such accumulation of NPs near the substrate was found to be useful to prevent the dewetting of the polystyrene films.[65] On the other hand, the AuNPs, in the PNC films containing semicrystalline P3HT, act as nucleating agents[66] to promote coil to rod conformational transition of the neighboring P3HT and the crystal growth. Accordingly, AuNP incorporated PNC (PN31 and PN11) thin films show enhanced crystallinity compared to the P3HT (PN30 and PN10) thin films. The positions of such AuNPs seem to play important role in the crystalline quality of P3HT and their orientation. AuNPs near the interfaces appear to assist the orientation of the crystallites other than edge-on and disturb the existing crystallites to deteriorate their backbone planarity. On the contrary, AuNPs present inside the P3HT matrix appear to promote the EO ordering and backbone planarity of the crystallites. The competitive effects of these two ultimately decide the faith of the effective EO ordering and the conjugation length in the film, namely deterioration of both the parameters in the PN31 film (effect of interfacial AuNPs only) and improvement of both the parameters in the PN11 film (dominating effect of dispersed AuNPs).

During TA of the PNC films, thermal energy promotes the diffusion of the AuNPs into the P3HT matrix, overcoming attraction from other AuNPs and repulsion from P3HT, to decrease the AuNP amount in the interfacial layers and improve the AuNP dispersion in the film. However, due to the semicrystalline nature of the P3HT matrix, the portion through which diffusion of AuNPs can take place is restricted.[24] This is because the separation between two backbone layers along alkyl side chains (∼1.6 nm) or $\pi-\pi$ stacking (∼0.38 nm) direction in the crystallites is less than the average size of the AuNPs, which restricts the AuNP diffusion through the crystalline P3HT aggregates. On the contrary, no such restriction is there in the amorphous region, rather its increase in the free volume with TA facilitates the AuNP diffusion into the P3HT matrix through the amorphous regions. In fact, any diffusion of AuNPs through the P3HT crystallites should give rise appreciable increase in the *d*-value (for diffusion within alkyl side chains) and noticeable deterioration in the crystallinity (for diffusion within $\pi-\pi$ stacking), which are not the case here. The lack of diffusion through crystallites and presence of diffusion through amorphous region, though limit but control the overall AuNP diffusion and dispersion. Such controlled dispersion of AuNPs in the amorphous region, through TA treatment, is further substantiated by the decrease in the film-thickness, which is quite useful to promote both the quantity (i.e., fraction or amount) and quality (i.e., planarity or conjugation length) of the P3HT crystallites and their connectivity.

From a thermodynamic point of view, the change in the free energy (ΔF) of a system is represented by

$$\Delta F = \Delta E - T\Delta S \tag{4}$$

where ΔE is the internal or enthalpic energy, ΔS is the entropic energy, and T is the temperature. A physical system tries to minimize its free energy to attend its thermodynamic stability, which can be through decreasing ΔE, i.e., by ordering or by increasing ΔS, i.e., disorder.[67,68] The formation of self-organized AuNP layers in the as-cast film indicates a dominant decrease of the enthalpic energy over entropy, while the dispersion of AuNPs in the film after TA indicates a dominant increase of the entropic energy over enthalpy. The thiol-coated AuNPs act as enthalpic NPs in P3HT system. Accordingly, in the as-cast film, the enthalpic interaction between AuNPs (i.e., organization) dominates over entropy (i.e., disorder). On the other hand, the thermal energy seems to weaken the enthalpic interaction (or organization) and to enhance the entropy (or disorder), which are quite useful even to disperse the enthalpic NPs in P3HT system.

The thermal energy also removes the thiol coatings of the AuNPs to promote their growth through agglomeration and coalesce of the nearby AuNPs,[55] as observed in the top surface.

https://doi.org/10.1021/acsapm.3c00049
ACS Appl. Polym. Mater. 2023, 5, 3359−3369

Such growth is counterproductive for NP dispersion, as the agglomerated large particles find themselves difficult to diffuse inside the polymer matrix. On the other hand, the removal of insulating thiol coatings from the dispersed AuNPs inside the polymer matrix is very productive or useful for creating better connectivity between crystallites. In fact, TA is a two-step process. During heating, the thermal energy promotes the diffusion and reorganization of the P3HT crystallites, the diffusion and dispersion of the AuNPs in the P3HT matrix and the removal of thiol coating from the dispersed AuNPs, while the subsequent cooling enhances the amount of the P3HT crystallites (through NP induced nucleation and growth), their planarity, conjugation length, EO ordering (through reorganization and compaction), and connectivity (through uncoated low resistive AuNPs). It can be noted that any presence of interaction between Au of AuNP and S of thiophene, which is difficult to substantiate from the present study, will further improve the connectivity. Such multidimensional improvement of structure and morphology of the PNC thin film should have a massive impact on their charge transport properties. Additionally, the large particles that are formed at the top surface due to TA can act as good top contact nanoelectrodes on the active layer (as the contact resistance and the charge injection barrier between such large particle and PNC layer are expected to be low) to create a good impact on the device properties. However, further work is required to visualize and validate the proposed structure of the PNC films directly using a microscopic technique such as cross-sectional transmission electron microscopy, to estimate the in-plane correlation of AuNPs, if any, using complementary X-ray scattering techniques such as grazing incidence small and wide-angle X-ray scattering, and finally to measure the device properties to correlate the properties with their structures.

CONCLUSIONS

The structures of the PNC thin films, incorporating AuNPs into P3HT, were studied using XR, AFM and optical absorption techniques to understand the organization and reorganization of AuNPs with TA and their effects on the crystallization and EO ordering of the P3HT matrix. The layering of AuNPs near the interfaces are evident in the as-cast PNC thin films, which can be correlated with the phase separation of the materials due to enthalpic interaction, i.e., strong interaction between similar materials and weak interaction between dissimilar materials. Further, the partially covered layer near the film−substrate interface (of near monolayer thickness) is found to be better confined compared to the film−air interface (of less than bilayer thickness), which can be attributed to the hard boundary condition of the substrate. The dispersion of AuNPs inside the P3HT matrix is evident after TA, which can be due to the thermal energy induced diffusion of AuNPs from the interfacial layers to amorphous P3HT regions (i.e., dominating entropic interaction overcoming enthalpic interaction). Further, the dispersion of AuNPs is found to enhance the crystallinity and EO ordering of the P3HT matrix. The enhancement of crystallinity can be realized considering NP-induced partial conversion of amorphous P3HT to crystallites, which can only happen if the dispersed-NPs are placed in the amorphous P3HT regions. Such understanding of NP dispersion in the semicrystalline polymer matrix and its ability to enhance the crystallinity, EO ordering, and connectivity of the semiconducting polymer, using proper complementary techniques, is very important to optimize the structure of the PNC for its better charge carrier mobility and device performances.

ASSOCIATED CONTENT

Supporting Information

The Supporting Information is available free of charge at https://pubs.acs.org/doi/10.1021/acsapm.3c00049.

Estimated size of AuNPs, EDP of a packed AuNP monolayer, variation in surface area and Minkowski volume, and simulated optical absorption spectra (PDF)

AUTHOR INFORMATION

Corresponding Author

Satyajit Hazra − *Saha Institute of Nuclear Physics, A CI of Homi Bhabha National Institute, Kolkata 700064, India;* orcid.org/0000-0001-5592-2078; Email: satyajit.hazra@saha.ac.in

Authors

Md Saifuddin − *Saha Institute of Nuclear Physics, A CI of Homi Bhabha National Institute, Kolkata 700064, India;* orcid.org/0000-0003-1416-3081

Arindam Biswas − *Saha Institute of Nuclear Physics, A CI of Homi Bhabha National Institute, Kolkata 700064, India*

Saugata Roy − *Saha Institute of Nuclear Physics, A CI of Homi Bhabha National Institute, Kolkata 700064, India*

Subhankar Mandal − *Saha Institute of Nuclear Physics, A CI of Homi Bhabha National Institute, Kolkata 700064, India*

Complete contact information is available at: https://pubs.acs.org/10.1021/acsapm.3c00049

Notes

The authors declare no competing financial interest.

ACKNOWLEDGMENTS

The authors thank Mr. G. Sarkar, Dr. B. Satpati, and Ms. S. Roy for their help in thin film preparations and TEM and UV−vis measurements, respectively, and Dr. J. R. Plaisier and Dr. L. Gigli for their co-operation in XR measurements at the MCX beamline. The financial support received from DST and Elettra under the Indo-Italian PoC to carry out XR experiments at Elettra is thankfully acknowledged. M.S. acknowledges the University Grant Commission (UGC), India, and A.B. and S.M. acknowledge the Council of Scientific & Industrial Research (CSIR), India, for providing research fellowships.

REFERENCES

(1) Coakley, K. M.; McGehee, M. D. Conjugated Polymer Photovoltaic Cells. *Chem. Mater.* **2004**, *16*, 4533−4542.

(2) Kim, Y.-H.; Yoo, B.; Anthony, J. E.; Park, S. K. Controlled Deposition of a High-Performance Small-Molecule Organic Single-Crystal Transistor Array by Direct Ink-jet Printing. *Adv. Mater.* **2012**, *24*, 497−502.

(3) Wang, M.; Baek, P.; Akbarinejad, A.; Barker, D.; Travas-Sejdic, J. Conjugated Polymers and Composites for Stretchable Organic Electronics. *J. Mater. Chem. C* **2019**, *7*, 5534−5552.

(4) Mandal, S.; Roy, S.; Saifuddin, M.; Hazra, S. Hole-Injection Barrier Across the Intermolecular Interaction Mediated Interfacial DNTT Layer. *Appl. Surf. Sci.* **2022**, *597*, 153696.

(5) Zen, A.; Pflaum, J.; Hirschmann, S.; Zhuang, W.; Jaiser, F.; Asawapirom, U.; Rabe, J. P.; Scherf, U.; Neher, D. Effect of Molecular Weight and Annealing of Poly(3-hexylthiophene)s on the Perform-

ance of Organic Field-Effect Transistors. *Adv. Funct. Mater.* **2004**, *14*, 757−764.
(6) Kline, R. J.; McGehee, M. D.; Kadnikova, E. N.; Liu, J.; Fréchet, J. M. J.; Toney, M. F. Dependence of Regioregular Poly(3-hexylthiophene) Film Morphology and Field-Effect Mobility on Molecular Weight. *Macromolecules* **2005**, *38*, 3312−3319.
(7) Choi, D.; Jin, S.; Lee, Y.; Kim, S. H.; Chung, D. S.; Hong, K.; Yang, C.; Jung, J.; Kim, J. K.; Ree, M.; et al. Direct Observation of Interfacial Morphology in Poly(3-hexylthiophene) Transistors: Relationship Between Grain Boundary and Field-Effect Mobility. *ACS Appl. Mater. Interfaces* **2010**, *2*, 48−53.
(8) Sirringhaus, H.; Brown, P. J.; Friend, R. H.; Nielsen, M. M.; Bechgaard, K.; Langeveld-Voss, B. M. W.; Spiering, A. J. H.; Janssen, R. A. J.; Meijer, E. W.; Herwig, P.; et al. Two-Dimensional Charge Transport in Self-Organized, High-Mobility Conjugated Polymers. *Nature* **1999**, *401*, 685−688.
(9) Duong, D. T.; Toney, M. F.; Salleo, A. Role of Confinement and Aggregation in Charge Transport in Semicrystalline Polythiophene Thin Films. *Phys. Rev. B* **2012**, *86*, 205205.
(10) Gargi, D.; Kline, R. J.; DeLongchamp, D. M.; Fischer, D. A.; Toney, M. F.; O'Connor, B. T. Charge Transport in Highly Face-on Poly(3-hexylthiophene) Films. *J. Phys. Chem. C* **2013**, *117*, 17421−17428.
(11) Roduner, E. Size Matters: Why Nanomaterials are Different. *Chem. Soc. Rev.* **2006**, *35*, 583−592.
(12) Klajn, R.; Stoddart, J. F.; Grzybowski, B. A. Nanoparticles Functionalised with Reversible Molecular and Supramolecular Switches. *Chem. Soc. Rev.* **2010**, *39*, 2203−2237.
(13) Manias, E. Stiffer by Design. *Nat. Mater.* **2007**, *6*, 9−11.
(14) Kumar, S. K.; Jouault, N.; Benicewicz, B.; Neely, T. Nanocomposites with Polymer Grafted Nanoparticles. *Macromolecules* **2013**, *46*, 3199−3214.
(15) Balazs, A. C.; Emrick, T.; Russell, T. P. Nanoparticle Polymer Composites: Where Two Small Worlds Meet. *Science* **2006**, *314*, 1107−1110.
(16) Akcora, P.; Liu, H.; Kumar, S. K.; Moll, J.; Li, Y.; Benicewicz, B. C.; Schadler, L. S.; Acehan, D.; Panagiotopoulos, A. Z.; Pryamitsyn, V.; et al. Anisotropic Self-Assembly of Spherical Polymer-Grafted Nanoparticles. *Nat. Mater.* **2009**, *8*, 354−359.
(17) Mackay, M. E.; Tuteja, A.; Duxbury, P. M.; Hawker, C. J.; Van Horn, B.; Guan, Z.; Chen, G.; Krishnan, R. S. General Strategies for Nanoparticle Dispersion. *Science* **2006**, *311*, 1740−1743.
(18) Chandran, S.; Begam, N.; Padmanabhan, V.; Basu, J. K. Confinement Enhances Dispersion in Nanoparticle−Polymer Blend Films. *Nat. Commun.* **2014**, *5*, 3697.
(19) A, N. D.; Swain, A.; Begam, N.; Bhattacharyya, A.; Basu, J. K. Temperature-Driven Grafted Nanoparticle Penetration into Polymer Melt: Role of Enthalpic and Entropic Interactions. *Macromolecules* **2020**, *53*, 8674−8682.
(20) Lin, Y.; Böker, A.; He, J.; Sill, K.; Xiang, H.; Abetz, C.; Li, X.; Wang, J.; Emrick, T.; Long, S.; et al. Self-Directed Self-Assembly of Nanoparticle/Copolymer Mixtures. *Nature* **2005**, *434*, 55−59.
(21) Gupta, S.; Zhang, Q.; Emrick, T.; Balazs, A. C.; Russell, T. P. Entropy-Driven Segregation of Nanoparticles to Cracks in Multilayered Composite Polymer Structures. *Nat. Mater.* **2006**, *5*, 229−233.
(22) Lee, D.; Sin, D. H.; Kim, S. W.; Lee, H.; Byun, H. R.; Mun, J.; Sung, W.; Kang, B.; Kim, D. G.; Ko, H.; et al. Singlet Exciton Delocalization in Gold Nanoparticle-Tethered Poly(3-hexylthiophene) Nanofibers with Enhanced Intrachain Ordering. *Macromolecules* **2017**, *50*, 8487−8496.
(23) Yi, C.; Yang, Y.; Liu, B.; He, J.; Nie, Z. Polymer-Guided Assembly of Inorganic Nanoparticles. *Chem. Soc. Rev.* **2020**, *49*, 465−508.
(24) Krauskopf, A. A.; Jimenez, A. M.; Altorbaq, A. S.; Müller, A. J.; Kumar, S. K. Quantifying Nanoparticle Ordering Induced by Polymer Crystallization. *ACS Nano* **2021**, *15*, 14430−14443.
(25) Huynh, W. U.; Dittmer, J. J.; Alivisatos, A. P. Hybrid Nanorod-Polymer Solar Cells. *Science* **2002**, *295*, 2425−2427.
(26) Lin, Y.-Y.; Chu, T.-H.; Li, S.-S.; Chuang, C.-H.; Chang, C.-H.; Su, W.-F.; Chang, C.-P.; Chu, M.-W.; Chen, C.-W. Interfacial Nanostructuring on the Performance of Polymer/TiO_2 Nanorod Bulk Heterojunction Solar Cells. *J. Am. Chem. Soc.* **2009**, *131*, 3644−3649.
(27) Wu, S.; Tai, Q.; Yan, F. Hybrid Photovoltaic Devices Based on Poly(3-hexylthiophene) and Ordered Electrospun ZnO Nanofibers. *J. Phys. Chem. C* **2010**, *114*, 6197−6200.
(28) Wang, C. C. D.; Choy, W. C. H.; Duan, C.; Fung, D. D. S.; Sha, W. E. I.; Xie, F.-X.; Huang, F.; Cao, Y. Optical and Electrical Effects of Gold Nanoparticles in the Active Layer of Polymer Solar Cells. *J. Mater. Chem.* **2012**, *22*, 1206−1211.
(29) Sun, Z.; Li, J.; Liu, C.; Yang, S.; Yan, F. Enhancement of Hole Mobility of Poly(3-hexylthiophene) Induced by Titania Nanorods in Composite Films. *Adv. Mater.* **2011**, *23*, 3648−3652.
(30) Raimondo, C.; Crivillers, N.; Reinders, F.; Sander, F.; Mayor, M.; Samorì, P. Optically Switchable Organic Field-Effect Transistors Based on Photoresponsive Gold Nanoparticles Blended with Poly(3-hexylthiophene). *Proc. Natl. Acad. Sci. U. S. A.* **2012**, *109*, 12375−12380.
(31) Han, S.-T.; Zhou, Y.; Yang, Q.-D.; Lee, C.-S.; Roy, V. A. L. Poly(3-hexylthiophene)/Gold Nanoparticle Hybrid System with an Enhanced Photoresponse for Light-Controlled Electronic Devices. *Part. Part. Syst. Charact.* **2013**, *30*, 599−605.
(32) Mosciatti, T.; Orgiu, E.; Raimondo, C.; Samorì, P. The Role of Size and Coating in Au Nanoparticles Incorporated into Bi-component Polymeric Thin-Film Transistors. *Nanoscale* **2014**, *6*, 5075−5080.
(33) Zhou, L.; Han, S.-T.; Zhuang, J.; Yan, Y.; Zhou, Y.; Sun, Q.-J.; Xu, Z.-X.; Roy, V. A. L. Mobility Enhancement of P3HT-Based OTFTs upon Blending with Au Nanorods. *Part. Part. Syst. Charact.* **2015**, *32*, 1051−1057.
(34) Grigorian, S.; Fontana, L.; Cerra, S.; Pietsch, U.; Scaramuzzo, F. A.; Fratoddi, I. Superior Transport Behavior of Gold Nanoparticles/P3HT Blends by Tuning Optical and Structural Properties. *Synth. Met.* **2022**, *283*, 116973.
(35) Saifuddin, M.; Mukhopadhyay, M.; Biswas, A.; Gigli, L.; Plaisier, J. R.; Hazra, S. Tuning the Edge-on Oriented Ordering of Solution-Aged Poly(3-hexylthiophene) Thin Films. *J. Mater. Chem. C* **2020**, *8*, 8804−8813.
(36) Saifuddin, M.; Roy, S.; Mandal, S.; Hazra, S. Vibronic States and Edge-on Oriented π-Stacking in Poly(3-alkylthiophene) Thin Films. *ACS Appl. Polym. Mater.* **2022**, *4*, 1377−1386.
(37) Parratt, L. J. Surface Studies of Solids by Total Reflection of X-rays. *Phys. Rev.* **1954**, *95*, 359−369.
(38) Gibaud, A.; Hazra, S. X-ray Reflectivity and Diffuse Scattering. *Curr. Sci.* **2000**, *78*, 1467−1477.
(39) Bal, J. K.; Hazra, S. Interfacial Role in Room-Temperature Diffusion of Au into Si Substrates. *Phys. Rev. B* **2007**, *75*, 205411.
(40) Chatterjee, P.; Hazra, S. The Hydrophilic/Hydrophobic Nature of a Cl-Terminated Si Surface. *Soft Matter* **2013**, *9*, 9799−9806.
(41) Mukhopadhyay, M.; Hazra, S. Interfacial and Thermal Energy Driven Growth and Evolution of Langmuir−Schaefer Monolayers of Au-Nanoparticles. *Phys. Chem. Chem. Phys.* **2018**, *20*, 1051−1062.
(42) Mukhopadhyay, M.; Hazra, S. Evolution of Ligand-Capped Nanoparticle Multilayers Toward a Near Unique Thickness. *Soft Matter* **2019**, *15*, 1869−1878.
(43) Roy, I.; Hazra, S. Solvent Dependent Ordering of Poly(3-dodecylthiophene) in Thin Films. *Soft Matter* **2015**, *11*, 3724−3732.
(44) Roy, I.; Hazra, S. Structures of Spin-Coated and Annealed Monolayer and Multilayer Poly(3-dodecylthiophene) Thin Films. *RSC Adv.* **2017**, *7*, 2563−2572.
(45) Roy, S.; Saifuddin, M.; Mandal, S.; Hazra, S. Stearic Acid Mediated Growth of Edge-on Oriented Bilayer Poly(3-hexylthiophene) Langmuir Films. *J. Colloid Interface Sci.* **2022**, *606*, 1153−1162.
(46) Spano, F. C.; Silva, C. H-and J-aggregate Behavior in Polymeric Semiconductors. *Annu. Rev. Phys. Chem.* **2014**, *65*, 477−500.
(47) Brust, M.; Walker, M.; Bethell, D.; Schiffrin, D. J.; Whyman, R. Synthesis of Thiol-Derivatised Gold Nanoparticles in a Two-Phase

Liquid−Liquid System. *J. Chem. Soc., Chem. Commun.* **1994**, *0*, 801−802.
(48) Mukhopadhyay, M.; Hazra, S. Growth of Thiol-Coated Au-Nanoparticle Langmuir Monolayers Through a 2D-network of Disk-like Islands. *RSC Adv.* **2016**, *6*, 12326−12336.
(49) Chatterjee, P.; Hazra, S.; Amenitsch, H. Substrate and Drying Effect in Shape and Ordering of Micelles Inside CTAB−Silica Mesostructured Films. *Soft Matter* **2012**, *8*, 2956−2964.
(50) Chatterjee, P.; Hazra, S. Time Evolution of a Cl-Terminated Si Surface at Ambient Conditions. *J. Phys. Chem. C* **2014**, *118*, 11350−11356.
(51) Roy, I.; Hazra, S. Poor Solvent and Thermal Annealing Induced Ordered Crystallites in Poly(3-dodecylthiophene) Films. *RSC Adv.* **2015**, *5*, 665−675.
(52) Mahato, S.; Puigdollers, J.; Voz, C.; Mukhopadhyay, M.; Mukherjee, M.; Hazra, S. Near 5% DMSO is the Best: A Structural Investigation of PEDOT: PSS Thin Films with Strong Emphasis on Surface and Interface for Hybrid Solar Cell. *Appl. Surf. Sci.* **2020**, *499*, 143967.
(53) Mandal, S.; Mukherjee, M.; Hazra, S. Evolution of Electronic Structures of Polar Phthalocyanine−Substrate Interfaces. *ACS Appl. Mater. Interfaces* **2020**, *12*, 45564−45573.
(54) Vignaud, G.; Gibaud, A. REFLEX: A Program for the Analysis of Specular X-ray and Neutron Reflectivity Data. *J. Appl. Crystallogr.* **2019**, *52*, 201−213.
(55) Meli, L.; Green, P. F. Aggregation and Coarsening of Ligand-Stabilized Gold Nanoparticles in Poly(methyl methacrylate) Thin Films. *ACS Nano* **2008**, *2*, 1305−1312.
(56) Sim, M.; Shin, J.; Shim, C.; Kim, M.; Jo, S. B.; Kim, J.-H.; Cho, K. Dependence of Exciton Diffusion Length on Crystalline Order in Conjugated Polymers. *J. Phys. Chem. C* **2014**, *118*, 760−766.
(57) Yamagata, H.; Spano, F. C. Interplay Between Intrachain and Interchain Interactions in Semiconducting Polymer Assemblies: The HJ-aggregate Model. *J. Chem. Phys.* **2012**, *136*, 184901.
(58) Clark, J.; Chang, J.-F.; Spano, F. C.; Friend, R. H.; Silva, C. Determining Exciton Bandwidth and Film Microstructure in Polythiophene Films Using Linear Absorption Spectroscopy. *Appl. Phys. Lett.* **2009**, *94*, 163306.
(59) Spano, F. C. Modeling Disorder in Polymer Aggregates: The Optical Spectroscopy of Regioregular Poly(3-hexylthiophene) Thin Films. *J. Chem. Phys.* **2005**, *122*, 234701.
(60) Clark, J.; Silva, C.; Friend, R. H.; Spano, F. C. Role of Intermolecular Coupling in the Photophysics of Disordered Organic Semiconductors: Aggregate Emission in Regioregular Polythiophene. *Phys. Rev. Lett.* **2007**, *98*, 206406.
(61) Nagarjuna, G.; Baghgar, M.; Labastide, J. A.; Algaier, D. D.; Barnes, M. D.; Venkataraman, D. Tuning Aggregation of Poly(3-hexylthiophene) within Nanoparticles. *ACS Nano* **2012**, *6*, 10750−10758.
(62) Manas, E. S.; Spano, F. C. Absorption and Spontaneous Emission in Aggregates of Conjugated Polymers. *J. Chem. Phys.* **1998**, *109*, 8087−8101.
(63) Roehling, J. D.; Arslan, I.; Moule, A. J. Controlling Microstructure in Poly(3-hexylthiophene) Nanofibers. *J. Mater. Chem.* **2012**, *22*, 2498−2506.
(64) Krishnan, R. S.; Mackay, M. E.; Duxbury, P. M.; Pastor, A.; Hawker, C. J.; Van Horn, B.; Asokan, S.; Wong, M. S. Self-Assembled Multilayers of Nanocomponents. *Nano Lett.* **2007**, *7*, 484−489.
(65) Barnes, K. A.; Karim, A.; Douglas, J. F.; Nakatani, A. I.; Gruell, H.; Amis, E. J. Suppression of Dewetting in Nanoparticle-Filled Polymer Films. *Macromolecules* **2000**, *33*, 4177−4177.
(66) Jabbarzadeh, A.; Halfina, B. Unravelling the Effects of Size, Volume Fraction and Shape of Nanoparticle Additives on Crystallization of Nanocomposite Polymers. *Nanoscale Adv.* **2019**, *1*, 4704−4721.
(67) Dai, X.; Hou, C.; Xu, Z.; Yang, Y.; Zhu, G.; Chen, P.; Huang, Z.; Yan, L.-T. Entropic Effects in Polymer Nanocomposites. *Entropy* **2019**, *21*, 186.
(68) Rocha, B. C.; Paul, S.; Vashisth, H. Role of Entropy in Colloidal Self-Assembly. *Entropy* **2020**, *22*, 877.

https://doi.org/10.1021/acsapm.3c00049
ACS Appl. Polym. Mater. 2023, 5, 3359−3369